Characterizing Enzyme Cooperativity with Imaging SAMDI-MS

Jennifer Grant+,[a] Blaise R. Kimmel+,[b] Lindsey C. Szymczak,[a] Juliet Roll,[c] and Milan Mrksich*[a, c]

Abstract: This paper describes a method that combines a microfluidic device and self-assembled monolayers for matrix-assisted laser desorption/ionization mass spectrometry (SAMDI) mass spectrometry to calculate the cooperativity in binding of calcium ions to peptidylarginine deiminase type 2 (PAD2). This example uses only 120 μL of enzyme solution and three fluidic inputs. This microfluidic device incorporates a self-assembled monolayer that is functionalized with a peptide substrate for PAD2. The enzyme and different concentrations of calcium ions are flowed through each of eight channels, where the position along the channel corresponds to reaction time and position across the channel corresponds to the concentration of Ca^{2+}. Imaging SAMDI (iSAMDI) is then used to determine the yield for the enzyme reaction at each 200 μm pixel on the monolayer, providing a time course for the reactions. Analysis of the peptide conversion as a function of position and time gives the degree of cooperativity (n) and the concentration of ligand required for half maximal activity ($K_{0.5}$) for the Ca^{2+} – dependent activation of PAD2. This work establishes a high-throughput and label-free method for studying enzyme-ligand binding interactions and widens the applicability of microfluidics and matrix-assisted laser desorption/ionization mass spectrometry (MALDI) imaging mass spectrometry.

Introduction

Cooperative binding interactions are important in enzyme activity, metabolic regulation, and cellular signaling. Binding of a metal or ligand to multiple sites in a protein is described by the Hill coefficient (n) which represents the degree of cooperativity and where $K_{0.5}$ describes the ligand concentration required for half maximal activity. Various methods – including X-ray crystallography,[1] isothermal titration calorimetry (ITC),[2] fluorescence polarization,[3] fluorescence resonance energy transfer (FRET),[4] and surface plasmon resonance (SPR)[5,6] – have been used to determine these parameters, but these methods remain challenging to adapt to particular enzyme reactions in biological samples due to low sensitivity and low-throughput.[7] Here, we demonstrate how the combination of microfluidic networks and iSAMDI-MS (imaging self-assembled monolayers for matrix-assisted laser desorption/ionization mass spectrometry) can be used to determine the Hill coefficient (n) and ligand concentration required for half-maximal activity ($K_{0.5}$) using iSAMDI-MS. This method allows us to perform and analyze thousands of reactions in a single experiment for calculating the Michaelis constant and rate of a chemical reaction.[8,9]

In this work, we characterize the Ca^{2+}-induced activation of peptidylarginine deiminase type 2 (PAD2), which catalyzes the hydrolysis of an arginine guanidinium group to the corresponding urea to give citrulline. PAD2 is involved in the progression of several diseases, including breast cancer,[10] rheumatoid arthritis,[11] and macular degeneration.[12] PAD2 is present in the cytoplasm[13] but requires calcium concentrations nearly 10-fold greater than intracellular levels for maximal activity.[1] Therefore, biochemical assays that measure PAD2 activation are important for studying its function and possible roles in disease progression. Several techniques have been developed to detect PAD-mediated citrullination and are important to our understanding of this enzyme family,[14–17] but rely on labels and secondary reporters, or are difficult to adapt towards high-throughput assays.[18] In the work that follows, we describe the development of high-throughput, low-volume assay with iSAMDI-MS to simultaneously analyze several hundred reaction conditions on one chip and show that PAD2 binds Ca^{2+} cooperatively with a n and $K_{0.5}$ value in agreement with established results from a prior study.[1]

Results and Discussion

We measured PAD2 activity using a peptide having an arginine residue in an optimal sequence context. The peptide is immobilized to a maleimide-terminated self-assembled mono-

[a] J. Grant,+ L. C. Szymczak, Prof. M. Mrksich
Department of Chemistry
Northwestern University
2145 Sheridan Rd, Evanston, IL, 60208 (USA)
E-mail: milan.mrksich@northwestern.edu

[b] B. R. Kimmel+
Department of Chemical and Biological Engineering
Northwestern University
2145 Sheridan Rd, Evanston, IL, 60208 (USA)

[c] J. Roll, Prof. M. Mrksich
Department of Biomedical Engineering
Northwestern University
2145 Sheridan Rd, Evanston, IL, 60208 (USA)

[+] These authors contributed equally to this manuscript.

Supporting information for this article is available on the WWW under https://doi.org/10.1002/chem.202103807

Chemistry–A European Journal

Research Article
doi.org/10.1002/chem.202103807

Chemistry Europe
European Chemical
Societies Publishing

layer (SAM) by way of reaction of a terminal cysteine residue with the maleimide group. PAD2 converts arginine to citrulline, which results in a mass increase of 0.98 Da in the citrulline product. This mass difference is challenging to reliably detect on a matrix-assisted laser desorption/ionization mass spectrometry (MALDI) mass spectrometer due to the generation of proton adducts of the peptide in the instrument. Thus, we first developed a quantitative assay to measure PAD2 enzyme activity that uses the serine protease trypsin to cleave the immobilized peptides at the arginine residue. In this way, when a peptide is treated with PAD2 followed by trypsin, only the unreacted peptide will be cleaved, leading to a significant mass difference with the (uncleaved) product (Figure 1).[19] To determine the peptide sequence for use in the assay, we generated a peptide library with the sequence Ac-G**XZ**RGC (**X** and **Z** denote all amino acids except cysteine, lysine, and arginine). We prepared an array from the 361 peptides and treated the array with PAD2 and then trypsin. We found that the sequence Ac-GYNRGC provided high PAD2 activity and good signal-to-noise with SAMDI-MS (Figure S1). We demonstrated that the trypsin detection strategy is quantitative by immobilizing known ratios of Ac-GYNRGC and Ac-GYNCitRGC and treating the surface with trypsin (Figure S3). We then calculated the percent of citrullinated peptide in the resulting spectra using the following equation [Equation (1)]:

$$\% \text{ citrullination} = [I_{Cit}/(I_{Cit} + I_R)] \times 100 \qquad (1)$$

where I_{Cit} is the intensity for the monoisotopic peak of the citrullinated peptide conjugated to the maleimide-alkanedisulfide and I_R is the intensity for the monoisotopic peak of the trypsinized peptide conjugated to the maleimide-alkanedisulfide. A linear response is observed with a slope of approximately 1.0 ($R^2 = 0.9961$), demonstrating that this method is quantitative. We observed no proteolysis when the immobilized citrullinated product was treated with trypsin, while the arginine-containing substrate underwent complete cleavage, as indicated by a decrease of 529 Da. Together, this demonstrates a high-throughput SAMDI-MS method for detecting PAD citrullination.

We next assembled a microfluidic device with two layers to generate a spatially resolved profile that gives kinetic information for distinct reaction times and concentrations of the metal cofactor and enzyme, based on a device that we described in an earlier report.[8] The device consists of two poly(dimethylsiloxane) (PDMS) fluidic layers. The enzyme is introduced in the top layer at 2.0 µL min⁻¹, where it is partitioned into eight identical and parallel channels (1.6 µM, in tris(2-carboxyethyl)phosphine hydrochloride at 200 µM). A buffer containing calcium ion (1.6 mM CaCl₂ in 100 mM Tris, pH 8.0, 50 mM NaCl) and a second buffer without calcium ion are introduced into two inlets in the bottom channel, both at 1.0 µL min⁻¹, where they go through a series of mixing steps to generate eight flows, each having a different concentration of calcium ion ranging from 0 to 800 µM (Figure 2). Each of the solutions containing enzyme are then brought into contact
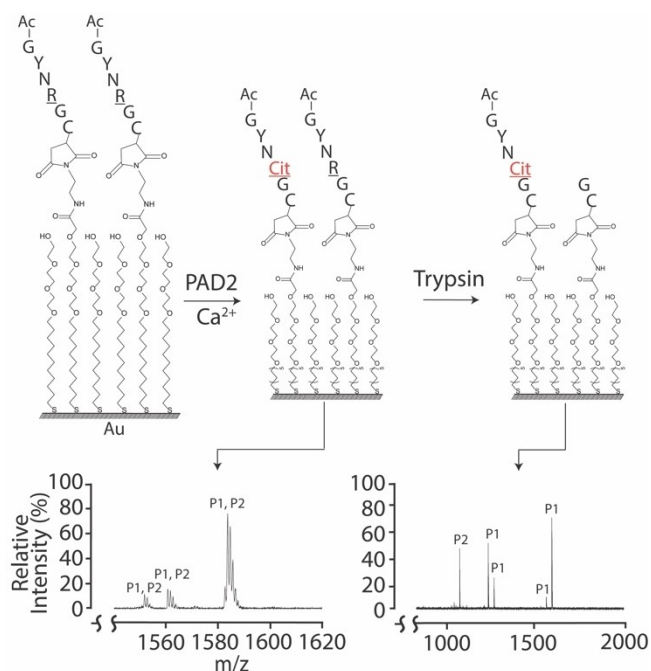

Figure 1. Assay for detecting PAD2 citrullination. The PAD2 peptide substrate (Ac-GYNRGC) is immobilized onto a self-assembled monolayer. The monolayer is treated with PAD2 and Ca²⁺. Subsequent treatment of the monolayer with trypsin reveals peaks representing the un-citrullinated, proteolyzed peptide (P2) and citrullinated peptide (P1).
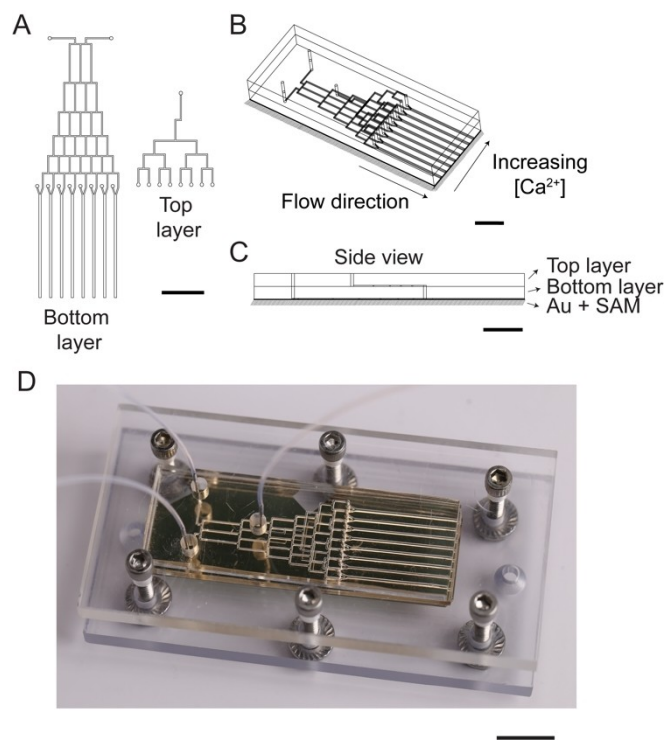

Figure 2. Microfluidic device layers and assembly with A) bottom view of both layers, B) the assembled device, and C) side view. D) Device and clamp assembly. All scale bars = 5 mm.

Chemistry–A European Journal

Research Article
doi.org/10.1002/chem.202103807

**Chemistry
Europe**
European Chemical
Societies Publishing

with one of the calcium ion solutions, which are then flowed down one of the eight channels in the device. The device was assembled with a monolayer floor, where the peptide was immobilized to an otherwise protein resistant surface at a density of approximately 10% against a background of tri(ethylene glycol)-terminated alkanethiolates. We found in previous work that a peptide density of 10% maintains inertness towards nonspecific protein adsorption to the surface and provides a sufficient amount of peptide for detection by SAMDI-MS.[8,9] Upon mixing of the solutions, the metal cofactor binds and activates the enzyme, which can then act on the immobilized peptide on the floor of the channel, leading to a conversion of the arginine residue to citrulline. Importantly, this device allows us to study the diffusion of Ca^{2+} into the enzyme fluidic channel, which creates a diffusion-mixing region and yields kinetic information on enzyme-metal cooperativity. We flowed the enzyme solution through the channel for one hour, after which the reaction was manually quenched with a rapid flow of EDTA (3 mM). The quenching was complete within seconds, and therefore does not impact the kinetics we measure. In this way, the position on the monolayer corresponds to a unique reaction time and calcium ion concentration. We then removed the microfluidic network, treated the monolayer with trypsin, and analyzed the monolayer with iSAMDI-MS to generate a spatial map of product yield, which was used to calculate n and $K_{0.5}$.

We acquired iSAMDI spectra in a 6.2 mm × 19.4 mm region on the chip at a pixel resolution of 200 μm. The resulting map contains a 31 × 97 array of pixels, where each pixel represents the yield of citrullinated product for a specific reaction time and calcium ion concentration (Figure 3A). As expected, in the absence of Ca^{2+}, no PAD2 activity is observed. Longer reaction times (i.e., greater distances from the Y-junction) and higher Ca^{2+} concentrations yield more citrullinated product, indicating a higher fraction of activated PAD2. No citrullination is observed in between the channels, indicating that trypsin uniformly cleaves the unmodified peptide, and that the device did not leak during operation. We also observe that enzyme activity at the start of the Y-junction, where the calcium and PAD2 solutions mix, favors the side of the channel supplying the enzyme. This is expected because the diffusion coefficients of Ca^{2+} and PAD2 are on the order of 10^{-5} cm^2 sec^{-1} [20] and 10^{-7} cm^2 sec^{-1},[21] respectively, and Ca^{2+} diffuses across the fluidic channel significantly faster than PAD2.

We averaged the product yield along the channel length and fitted the yield in GraphPad Prism to a Hill cooperative binding model[1] to obtain maximum reaction rate (V_{max}), n, and $K_{0.5}$ [Equation (2)]:

$$v_0 = V_{max} * [Ca^{2+}]^n / (K_{0.5}^n + [Ca^{2+}]^n) \qquad (2)$$

where v_0 is the rate of reaction to form the citrullinated product (% yield per minute) and $[Ca^{2+}]$ is the concentration of calcium. We repeated the experiment three times to obtain $V_{max} = 1.9 \pm 0.2$% yield/minute, $n = 3.5 \pm 1.1$ and $K_{0.5} = 240 \pm 30$ μM, demonstrating positive cooperativity for binding between calcium and PAD2 in arginine citrullination (Figure 3B–C). Thompson and
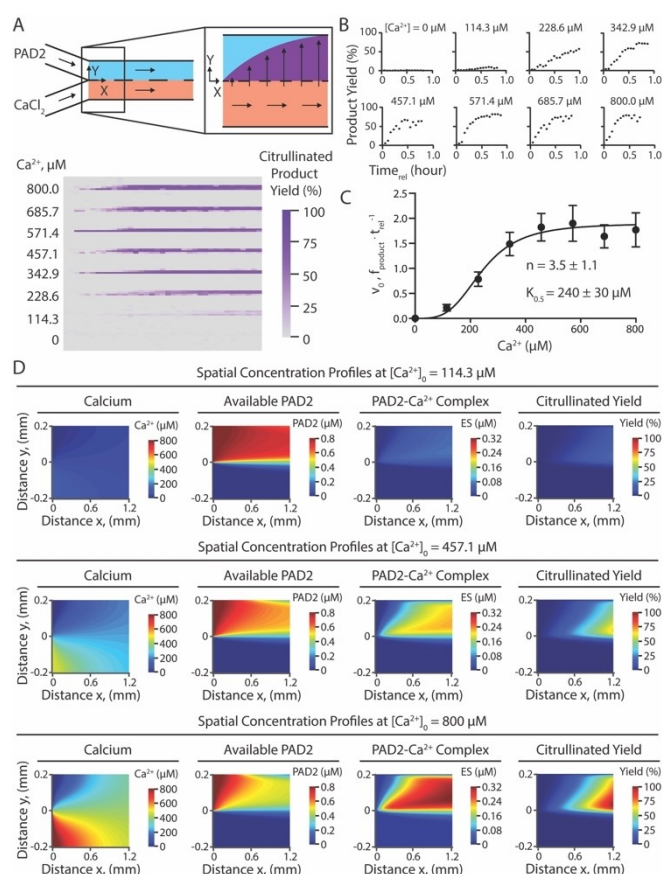

Figure 3. A) Illustration of calcium dispersion into the enzyme-rich fluid regime and spatial map of PAD2 citrullination at each x,y- coordinate (31 × 97-pixel array). B) Representative initial rate curves from each channel. The data is plotted as a function of relative time, or time$_{rel}$, in the channel due to dispersion. C) Hill plot from 3 experimental replicates, $R^2 = 0.65$. The initial rate of reaction, v_0, is plotted as the percent of citrullinated product over relative time, % min^{-1}. Error shown as the standard error of the mean (SEM). D) Simulated steady-state spatial concentration profiles at the Y-junction of the microfluidic device, as shown in subfigure A. Plots show numerical calculations at three concentrations of calcium within the x,y-plane of the device. Heat maps represent concentrations of calcium, enzyme, or the enzyme-metal complex, as well as citrullinated product in percent yield.

coworkers previously reported a value of n between 3.3 to 3.8 and $K_{0.5} = 250 \pm 15$ μM, which agrees with the results of our cooperative binding model.[1] Similar binding kinetics were also observed in a different study on PAD4, showing convergence within the PAD enzyme family.[22]

We next used numerical calculations to build a finite element model to describe the spatiotemporal pattern of reaction yields within the microfluidic device. Our approach was based on previous studies that modeled a steady-state reaction-diffusion network that incorporated the velocity pressure-driven fluid front, as well as the diffusion of all soluble species for calculating spatial concentration profiles.[9,23] In this work, we simulated the spatial concentration profiles of Ca^{2+}, PAD2, the intermediate PAD2-Ca^{2+} complex, and the citrullinated product in an x,y-plane in the center of the channel. It is important to note that we neglected the height of the device,

Chemistry–A European Journal

Research Article
doi.org/10.1002/chem.202103807

Chemistry
Europe
European Chemical
Societies Publishing

which simplified the transport of fluid to only two dimensions and assumes no diffusion of the immobilized peptide. Using the calculated kinetic parameters and the Hill coefficient, we calculated spatial-concentration profiles for all species along a gradient of Ca^{2+} concentrations in the diffusion-mixing region of the device (Figure 3D). The simulated heatmaps agree well with the experimentally determined yields of citrullinated product by iSAMDI-MS, as seen when comparing the maximum citrullinated yields for each concentration of calcium in Figure 3B and Figure 3D (with approximate yields of 10% at $[Ca^{2+}]=114.3$ μM, 60% at $[Ca^{2+}]=457.1$ μM, and 100% at $[Ca^{2+}]=800$ μM). Combined with the quantitative iSAMDI-MS analysis, this modeling approach presents a simple method for designing, simulating, and visualizing cofactor-mediated binding kinetics within microfluidic devices.

Conclusions

In this paper, we describe a high-throughput strategy based on microfluidics and iSAMDI-MS to characterize the degree of cooperativity and $K_{0.5}$ of a cooperative binding interaction. A microfluidic device with two layers and just 3 fluidic inputs allows thousands of discrete experiments to be performed, and that are sufficient to characterize the cooperativity of Ca^{2+}-PAD2 binding. In this example only 120 μL of the enzyme solution and a reaction time of one hour were required. The fluid flow rate and iSAMDI-MS pixel resolution allowed us to calculate the initial rate of formation before the reaction reached saturation. Faster reactions can be studied by increasing the fluid flow rate or decreasing the MALDI pixel resolution.[24] In this work, 93 data points were collected from each channel with a 200 μm pixel resolution. The pixel count can be increased using commercial MALDI mass spectrometers capable of imaging at a pixel resolution of 10 μm (rapifleX MALDI Tissuetyper, Bruker Daltonics).[25] The use of SAMDI mass spectrometry also has the benefit of providing a *direct readout* of enzyme activity. Further, iSAMDI-MS is not limited to peptides, but can also be used with small molecules, proteins, and carbohydrate substrates. In comparison to other cooperativity assays, the flexibility inherent to iSAMDI-MS and the high-throughput performance of the technique make it particularly well-suited for parallelization, which may find applications in enzyme library screening and drug discovery. Finally, our finite element model agreed well with the experimental data and is particularly useful in analyzing complex spatiotemporal data. The high-throughput label-free assay we describe for measuring PAD2 activity will have broader utility.[26] We envision that this methodology will have great use in high-throughput screening applications and will be extended towards other complex methods of activation in biology such as proteolysis,[27] protein-protein binding,[28] and prodrug activation.[29]

Experimental Section

See Supporting Information.

Conflict of Interest

The authors declare no conflict of interest.

Data Availability Statement

The data that support the findings of this study are available from the corresponding author upon reasonable request.

[1] D. J. Slade, P. Fang, C. J. Dreyton, Y. Zhang, J. Fuhrmann, D. Rempel, B. D. Bax, S. A. Coonrod, H. D. Lewis, M. Guo, et al., *ACS Chem. Biol.* **2015**, *10*, 1043–1053.
[2] A. Brown, *Int. J. Mol. Sci.* **2009**, *10*, 3457–3477.
[3] A. M. Rossi, C. W. Taylor, *Nat. Protoc.* **2011**, *6*, 365–387.
[4] D. C. Braun, S. H. Garfield, P. M. Blumberg, *J. Biol. Chem.* **2005**, *280*, 8164–8171.
[5] M. C. Jecklin, S. Schauer, C. E. Dumelin, R. Zenobi, *J. Mol. Recognit.* **2009**, *22*, 319–329.
[6] T. W. Herling, D. J. O'Connell, M. C. Bauer, J. Persson, U. Weininger, T. P. J. Knowles, S. Linse, *Biophys. J.* **2016**, *110*, 1957–1966.
[7] M. Choi, J.-S. Song, H.-J. Kim, S. Cha, E. Y. Lee, *Anal. Biochem.* **2013**, *437*, 62–67.
[8] J. Grant, S. H. Goudarzi, M. Mrksich, *Anal. Chem.* **2018**, *90*, 13096–13103.
[9] J. Grant, P. T. O'Kane, B. R. Kimmel, M. Mrksich, *ACS Cent. Sci.* **2019**, *5*, 586–493.
[10] S. Haribata, K. E. Rogers, D. Sadegh, L. J. Anguish, J. L. McElwee, P. Shah, P. R. Thompson, S. A. Coonrod, *BMC Cancer* **2017**, *17*, 378.
[11] D. Damgaard, L. Senolt, C. H. Nielsen, *Rheumatology* **2016**, *55*, 918–927.
[12] V. L. Bonilha, K. G. Shadrach, M. E. Rayborn, Y. Li, G. J. T. Pauer, S. A. Hagstrom, S. K. Bhattacharya, J. G. Hollyfield, *Exp. Eye Res.* **2013**, *111*, 71–78.
[13] E. Darrah, A. Rosen, J. T. Giles, F. Andrade, *Ann. Rheum. Dis.* **2012**, *71*, 92–98.
[14] M. Knipp, M. Vasák, *Anal. Biochem.* **2000**, *286*, 257–264.
[15] J. Fert-Bober, J. T. Giles, R. J. Holewinski, J. A. Kirk, H. Uhrigshardt, E. L. Crowgey, F. Andrade, C. O. Bingham, J. K. Park, M. K. Halushka, et al., *Cardiovasc. Res.* **2015**, *108*, 232–242.
[16] K. W. Clancy, E. Weerapana, P. R. Thompson, *Curr. Opin. Chem. Biol.* **2016**, *30*, 1–6.
[17] E. A. V. Moelants, J. Van Damme, P. Proost, *PLoS One* **2011**, *6*, e28976.
[18] K. L. Bicker, V. Subramanian, A. A. Chumanevich, L. J. Hofseth, P. R. Thompson, *J. Am. Chem. Soc.* **2012**, *134*, 17015–17018.
[19] E. Wildeman, M. M. Pires, *ChemBioChem* **2013**, *14*, 963–967.
[20] R. A. Robinson, C. L. Chia, *J. Am. Chem. Soc.* **1952**, *74*, 2776–2777.
[21] M. E. Young, P. A. Carroad, R. L. Bell, *Biotechnol. Bioeng.* **1980**, *22*, 947–955.
[22] Y.-L. Liu, Y.-H. Chiang, G.-Y. Liu, H.-C. Hung, *PLoS One* **2011**, *6*, e21314.
[23] W. D. Ristenpart, J. Wan, H. A. Stone, *Anal. Chem.* **2008**, *80*, 3270–3276.
[24] K. P. Nichols, S. Azoz, H. J. G. E. Gardeniers, *Anal. Chem.* **2008**, *80*, 8314–8319.

[25] A. Zavalin, J. Yang, K. Hayden, M. Vestal, R. M. Caprioli, *Anal. Bioanal. Chem.* **2015**, *407*, 2337–2342.

[26] D. M. Lewallen, K. L. Bicker, F. Madoux, P. Chase, L. Anguish, S. Coonrad, P. Hodder, P. R. Thompson, *ACS Chem. Biol.* **2014**, *9*, 913–921.

[27] P. Chakraborty, L. Acquasaliente, L. A. Pelc, E. D. Cera, *Sci. Rep.* **2018**, *8*, 4080.

[28] B. E. Hall, D. Bar-Sagi, N. Nassar, *Proc. Natl. Acad. Sci. USA* **2002**, *99*, 12138–12142.

[29] R. Peri-Naor, T. Ilani, L. Motiei, D. Margulies, *J. Am. Chem. Soc.* **2015**, *137*, 9507–9510.